



Geofísica internacional

ISSN: 0016-7169

Instituto de Geofísica, UNAM

Teja-Juárez, V. Leonardo; Cruz, Luis M. de la  
A Graphic Processing Unit (GPU) based implementation of  
an incompressible two-phase flow model in porous media  
Geofísica internacional, vol. 57, no. 3, 2018, July-September, pp. 205-222  
Instituto de Geofísica, UNAM

Available in: <https://www.redalyc.org/articulo.oa?id=56871786005>

- How to cite
- Complete issue
- More information about this article
- Journal's webpage in redalyc.org

UNAM  
redalyc.org

Scientific Information System Redalyc

Network of Scientific Journals from Latin America and the Caribbean, Spain and Portugal

Project academic non-profit, developed under the open access initiative

# A Graphic Processing Unit (GPU) based implementation of an incompressible two-phase flow model in porous media

V. Leonardo Teja-Juárez\* and Luis M. de la Cruz

Received: March 14, 2018; accepted: May 23, 2018; published on line: July 02, 2018

## Resumen

En este trabajo se presenta una estrategia de paralelización de un simulador completamente implícito para la solución numérica del modelo de flujo bifásico incompresible en medios porosos usando unidades de procesamiento gráfico (GPU, por sus siglas en inglés). El modelo matemático está basado en las ecuaciones de conservación de masa para las fases agua y aceite. Se utiliza la formulación Presión-Saturación para simplificar el modelo numérico. La técnica de Volumen Finito y el método de Newton-Raphson se usan para discretizar y linealizar las ecuaciones diferenciales parciales, respectivamente. Se propone la construcción del Jacobiano directamente en la GPU, lo que reduce la información que debe intercambiarse entre la CPU (Unidad Central de Procesamiento CPU, por sus siglas en inglés) y la GPU. El simulador utiliza bibliotecas que ya incluyen los métodos del subespacio de Krylov para resolver sistemas de ecuaciones lineales. Se comparan los resultados de tres problemas de referencia utilizando diferentes tamaños de malla. También se evalúa el rendimiento del código numérico desarrollado. Los resultados de la GPU versus CPU indican que el simulador numérico alcanzó hasta 22x de aceleración para construir el Jacobiano y 3x de aceleración para ejecutar el código numérico completo usando la paralelización GPU.

Palabras clave: Modelo bifásico, Newton-Raphson, Unidades de Procesamiento Gráfico (GPU), construcción del Jacobiano, aceleración.

## Abstract

In this paper a parallelization strategy of a fully implicit simulator for the numerical solution of the incompressible two-phase flow model in porous media is presented using GPUs (Graphics Processing Units). The mathematical model is based on the mass conservation equations for the water and oil phases. Mathematical formulation of Pressure-Saturation is used to simplify the numerical model. The Finite Volume technique and the Newton-Raphson method are used to discretize and linearize the partial differential equations, respectively. The construction of the Jacobian directly on the GPU is proposed, which reduces the information that needs to be exchanged between the CPU (Central Processing Unit) and the GPU. The simulator uses libraries that already include methods that belong to the Krylov subspace to solve linear equations systems. The results of three benchmark problems by using different grid sizes are compared. The performance of the numerical code developed is also evaluated. Results of the GPU against the CPU indicate that the numerical simulator reached 22x of speed up to build the Jacobian, and 3x of speed up for executing the whole numerical code by using the GPU parallelization.

Key words: Two-phase flow model, Newton-Raphson, Graphics Processing Units (GPU), Jacobian construction, speed up.

---

V. L. Teja-Juárez\*  
Posgrado en Ciencias de la Tierra  
Universidad Nacional Autónoma de México  
Ciudad universitaria  
Delegación Coyoacán, 04510  
México CDMX, México  
\*Corresponding author: vleonardo.teja@gmail.com

L. M. de la Cruz  
Instituto de Geofísica  
Universidad Nacional Autónoma de México  
Ciudad universitaria  
Delegación Coyoacán, 04510  
México CDMX, México

## Introduction

Nowadays new techniques called Enhanced Oil Recovery Methods (EOR) are applied to improve the oil recovery in a hydrocarbon reservoir. Lake (1989) gives a definition for the EOR methods: EOR is oil recovery by the injection of materials not normally present in the reservoir. This definition covers all modes of oil recovery and most oil recovery agents. Considering this definition the EOR methods might consider both secondary and tertiary recovery. Before EOR methods are applied there is a technique that almost always has to be considered, that is, the waterflooding technique. Waterflooding technique is the oldest assisted recovery method and it remains as the most common method used to sweep the oil that was not produced by natural pressure, and to keep the oil pressure when this has declined due to reservoir conditions (Latil, 1980). On the other hand, due to the growing need in the oil industry to make faster and more efficient calculations to simulate the recovery conditions before, during and after the production life of a reservoir, it is necessary to test new computational techniques that reduce the run time of the numerical simulators. Several investigations have been carried out to improve the run time of the reservoir simulators (Killough *et al.*, 1991; Shiralkar *et al.*, 1998; Ma and Chen, 2004; Dogru *et al.*, 2009). Most of these papers have been developed using distributed computing. Recently, Wang *et al.* (2015) developed a scalable black oil simulator using ten millions of grid blocks approximately, their simulator reached a scalability factor of 1.03 using 2048 processors. Also Liu *et al.* (2015) developed a three phase parallel simulator applying MPI (Message Passing Interface) for communications between computational nodes and OpenMP for shared memory. They obtained an efficiency of 95.7% by using 3072 processors. However, there is a limitation to use this technique, since a computational cluster with tens until thousands of processors is needed to achieve the desired speed up.

As an alternative NVIDIA has developed a programming language called CUDA (Compute Unified Device Architecture) which can be used to take advantage of the power computing graphics cards for general purpose simulations. Yu *et al.* (2012), used GPUs to parallelize a reservoir simulator which can run large scale problems. They used over one million grid blocks obtaining a good speed up compared to the numerical code of the CPU. Li and Saad (2013), developed a numerical code of preconditioned linear solvers based on GPU, their numerical experiments indicate that Incomplete LU (ILU)

factorization preconditioned GMRES method achieved a speed up nearing to 4 compared versus CPU numerical code. Liu *et al.* (2013), reported improved preconditioners and algebraic multigrid linear solvers applied to reservoir simulations using GPUs. De la Cruz and Monsivais (2014) developed a two phase porous media flow simulator to compare the performance of a single GPU with a single node of a cluster using distributed memory. These authors found that a single GPU is better than a computational node with twelve processors. Trapeznikova *et al.* (2014) developed a software library for numerical simulation of multiphase porous media flows that is applied to GPU-CPU hybrid supercomputers. The model is implemented by an original algorithm of the explicit type. An explicit three-level approximation of the modified continuity equation is used. After that the Newton method is used locally at each point of the computational grid. Authors used SPE-10 project as benchmark, they achieved a 97x of speed up when they compare the run time obtained by a single GPU versus one CPU, and 18x of speed up when a computational node of six processors is used. Mukundakrishnan *et al.* (2015), presented the implementation in GPUs of a black oil simulator, which uses a fully implicit scheme for the discretization in the time and the constrained pressure residual -algebraic multigrid (CPR-AMG) to solve the linear system equations. They reported an average of 20 minutes for the run time to solve a problem with 16 million of active blocks by using 4 GPUs. Anciaux-Sedrakian *et al.* (2015) made a numerical study of different preconditioners such as: Polynomial, ILU and CPR-AMG which were implemented in a heterogeneous architecture (CPU-GPU). They emphasize two key points to obtain high performance in heterogeneous architectures; the first is to maximize the utilization and occupancy of the GPU and the second refers to minimize the high cost of transferring GPU data to the node with the CPUs and vice versa. Their results show that a combination of 1 processor plus 1 GPU is approximately 2 times faster compared versus an 8-processor node by applying CPR-AMG preconditioner.

In this work a simulator for oil recovery was developed based in the water injection process and the simultaneous solution technique described by Chen *et al.* (2006). A parallelization scheme is proposed by using GPUs for both the construction of the Jacobian matrix and the solution of the linear system of equations.

The paper is organized in this way: In Section 2, the mathematical equations of the water injection and pressure-saturation

formulation model are introduced. In Section 3, the numerical discretization is presented by using the Finite Volume Method (FVM) and the linearization of the equations by applying the Newton-Raphson method (NR). In Section 4, the computational implementation of the CPU and GPU are shown and main algorithms are explained. In Section 5, numerical results of three benchmark problems are presented. Also in this section, the performance of the parallel numerical code is evaluated by comparing the run time obtained in both GPU and CPU.

### Mathematical model of the incompressible two-phase flow in porous media

The mathematical model of the incompressible two-phase flow can be used to simulate the water injection into a hydrocarbon reservoir. The mass balances are obtained by taking into account two phases: oil and water. Governing equations can be obtained by applying an axiomatic formulation (see Herrera and Pinder, 2012 for a complete description on this formulation). A general local balance mass equation can be written as follows:

$$\frac{\partial(\phi \rho_\alpha S_\alpha)}{\partial t} + \nabla \cdot (\vec{u}_\alpha \rho_\alpha) = q_\alpha \quad (1)$$

Here  $\phi$  is the porosity of the media  $\rho_\alpha$ ,  $S_\alpha$ ,  $\vec{u}_\alpha$  and  $q_\alpha$  represent the density, saturation, velocity and source of phase  $\alpha$ . The Darcy's velocity is used expressed as follows:

$$\vec{u}_\alpha = -\frac{\bar{k} k_{r\alpha}}{\mu_\alpha} \nabla \Phi_\alpha \quad (2)$$

where  $\bar{k}$  is the diagonal tensor of absolute permeability and  $k_{r\alpha}$  is the relative permeability of phase  $\alpha$ ; the Greek letters  $\Phi_\alpha$  and  $\mu_\alpha$  are the potential and the dynamic viscosity for phase  $\alpha$ , respectively. Now, substituting (2) into (1) and replacing  $\alpha$  by  $o$  and  $w$ , the next two coupled mass balance equations were obtained (Chen *et al.*, 2006):

$$\frac{\partial \phi \rho_w S_w}{\partial t} = \nabla \cdot \left( \frac{\bar{k} k_{rw} \rho_w}{\mu_w} \nabla \Phi_w \right) + q_w \quad (3)$$

$$\frac{\partial \phi \rho_o S_o}{\partial t} = \nabla \cdot \left( \frac{\bar{k} k_{ro} \rho_o}{\mu_o} \nabla \Phi_o \right) + q_o \quad (4)$$

The mass balance equations are interrelated by the following mathematical expressions:

$$S_o + S_w = 1 \quad (5)$$

$$\Phi_\alpha + \rho_\alpha - \rho_w \wp z \quad (6)$$

$$p_w = p_o - p_{cow} \quad (7)$$

$$p_{cow} = p_{cow}(S_w) \quad (8)$$

where  $p_\alpha$  is the pressure of the phase  $\alpha$ ,  $\wp$  is the magnitude of gravity,  $z$  is the depth and  $p_{cow}$  is the oil-water capillary pressure as a function of  $S_w$ .

Equations (3) and (4) are non-linear and strongly coupled. In order to simplify the numerical solution of these equations, the pressure-saturation formulation was used which consists in selecting oil pressure and water saturation as primary variables and in using the fractional flow theory to derive one equation for pressure and one equation for saturation (Peaceman, 1977; Chen *et al.*, 2006). The mass balance equation for water phase is:

$$\frac{\partial(\phi \rho_w S_w)}{\partial t} - \nabla \cdot \left( \rho_w \frac{\bar{k} k_{rw}}{\mu_w} ((\nabla p_o - \nabla p_{cow}) - \rho_w \wp \nabla z) \right) = q_w \quad (9)$$

Considering non-compressible flow, equation (9) becomes:

$$\phi \frac{\partial S_w}{\partial t} - \nabla \cdot \left[ \bar{k} \lambda_w \cdot \left( \nabla p_o - \frac{dp_{cow}}{dS_w} \nabla S_w - \rho_w \wp \nabla z \right) \right] = \frac{q_w}{\rho_w} \quad (10)$$

where the following substitutions were carried out:

$$\nabla p_{cow} = \frac{dp_{cow}}{dS_w} \nabla S_w \quad (11)$$

$$\lambda_w = \frac{k_{rw}}{\mu_w} \quad (12)$$

Taking into account the fractional flow of the phase  $\alpha$  ( $f_\alpha$ ) that is defined as the quotient of the phase  $\alpha$  mobility ( $\lambda_\alpha$ ) over the total mobility ( $\lambda$ ),  $f_\alpha = \frac{\lambda_\alpha}{\lambda}$ , a general pressure equation was derived:

$$\frac{\partial \phi}{\partial t} - \nabla \cdot \bar{k} \lambda \left[ \sum_{\alpha} f_{\alpha} \nabla p_{\alpha} - \sum_{\alpha} f_{\alpha} \rho_{\alpha} \phi \nabla z \right] + \sum_{\alpha} \frac{1}{\rho_{\alpha}} \left[ \phi S_{\alpha} \frac{\partial \rho_{\alpha}}{\partial t} + \bar{u}_{\alpha} \nabla \cdot \rho_{\alpha} \right] - \sum_{\alpha} \frac{q_{\alpha}}{\rho_{\alpha}} = 0 \quad (13)$$

For more details about fractional flow formulation readers can consult Chen *et al.*, 2006. Considering no change in the porosity, and non-compressible flows, equation (13) can be reduced to:

$$-\nabla \cdot \left[ \bar{k} \lambda \nabla p_o - \bar{k} \lambda_w \frac{dp_{cow}}{dS_w} \nabla S_w - (\lambda_o \rho_o + \lambda_w \rho_w) \phi \nabla z \right] = \frac{q_w}{\rho_w} + \frac{q_o}{\rho_o} \quad (14)$$

Equations (10) and (14) are coupled and non-linear. The Newton-Raphson approach was used to linearize the equations and solve them using a fully-implicit strategy. In this work three different cases of study are described.

### Numerical model

In this section a brief description is given of the use of the Finite Volume Method (FVM) to discretize equations (10) and (14), and the

Newton-Raphson method to linearize those equations.

#### Calculation of residuals by using the Finite Volume Method

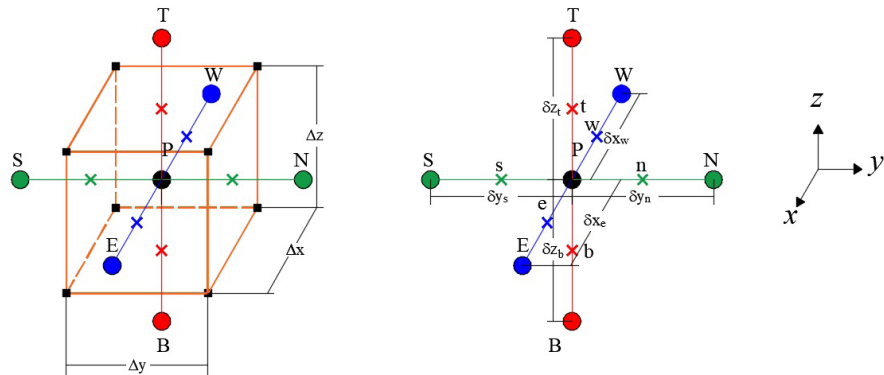
As a way to show how FVM is applied to compute the residuals for the governing equations, the saturation equation for the three-dimensional case is discretized. Integrating equation (10) with respect to time and the control volume shown in Figure 1, equation (15) is obtained:

$$\int_n^{n+1} \left\{ \int_{\Delta V} \left[ \phi \frac{\partial S_w}{\partial t} - \nabla \cdot \left[ \bar{k} \lambda_w \left( \nabla p_o - \frac{dp_{cow}}{dS_w} \nabla S_w - \rho_w \phi \nabla z \right) \right] - \frac{q_w}{\rho_w} \right] dV \right\} dt = 0 \quad (15)$$

In order to evaluate the terms of equation (15) the following considerations were taken into account: 1) a backward Euler approximation is used, 2) the permeability tensor is diagonal and 3) the space derivatives are approximated using central differences. Therefore, the discretized form of equation (15) in terms of a residual is written as follows:

$$\begin{aligned} R_w(p_o, S_w) = & \frac{\phi \Delta V}{\Delta t} [(S_w)_n - (S_w)_P] - [T_{w,e}(p_{o,e} - p_{o,P}) - T_{w,w}(p_{o,P} - p_{o,W})] + [T_{w,e} \frac{dp_{cow}}{dS_w} \Big|_e (S_{w,e} - S_{w,P}) \\ & - T_{w,w} \frac{dp_{cow}}{dS_w} \Big|_w (S_{w,P} - S_{w,W})] + [T_{w,e} \phi \rho_w \Big|_e (z_{w,e} - z_{w,P}) - T_{w,w} \phi \rho_w \Big|_w (z_{w,P} - z_{w,W})] \\ & - [T_{w,n}(p_{o,n} - p_{o,P}) - T_{w,s}(p_{o,P} - p_{o,S})] + [T_{w,n} \frac{dp_{cow}}{dS_w} \Big|_n (S_{w,n} - S_{w,P}) \\ & - T_{w,s} \frac{dp_{cow}}{dS_w} \Big|_s (S_{w,P} - S_{w,S})] + [T_{w,n} \phi \rho_w \Big|_n (z_{w,n} - z_{w,P}) - T_{w,s} \phi \rho_w \Big|_s (z_{w,P} - z_{w,S})] \\ & - [T_{w,t}(p_{o,t} - p_{o,P}) - T_{w,b}(p_{o,P} - p_{o,B})] + [T_{w,t} \frac{dp_{cow}}{dS_w} \Big|_t (S_{w,t} - S_{w,P}) \\ & - T_{w,b} \frac{dp_{cow}}{dS_w} \Big|_b (S_{w,P} - S_{w,B})] + [T_{w,t} \gamma_w \Big|_t (z_{w,t} - z_{w,P}) - T_{w,b} \gamma_w \Big|_b (z_{w,P} - z_{w,B})] - \frac{q_{w,P}}{\rho_w} \Delta V \end{aligned} \quad (16)$$

**Figure 1.** Three-dimensional stencil to apply the FVM.  $\Delta V = \Delta x \Delta y \Delta z$  is defined.



where the transmissibility is computed as  $T_w = \frac{k_{ii} \lambda_w A_i}{\delta x_i}$  for  $i=1, 2, 3$ ; the specific weight is defined as  $\gamma_w = \rho_w g$ ,  $A_i$  is the face area of volume perpendicular to the axis  $i$ , for example,  $A_1 = \Delta y \Delta z$ , and  $\delta x_i$  represents the distance between neighboring volumes centers. Similarly the residual  $R_o$  for the pressure equation (14), is expressed as follows:

$$\begin{aligned}
 R_o(p_o, S_w) = & [T_e(p_{o,E} - p_{o,P}) - T_w(p_{o,P} - p_{o,W})] - [T_{w,e} \frac{dp_{cow}}{dS_w} \Big|_e (S_{w,E} - S_{w,P}) - T_{w,w} \frac{dp_{cow}}{dS_w} \Big|_w (S_{w,P} - S_{w,W})] \\
 & - [\frac{k_{xx}(\lambda_w \gamma_w + \lambda_o \gamma_o) A_1}{\delta x} \Big|_e (z_{w,E} - z_{w,P}) - \frac{k_{xx}(\lambda_w \gamma_w + \lambda_o \gamma_o) A_1}{\delta x} \Big|_w (z_{w,P} - z_{w,W})] \\
 & + [T_{w,n} (p_{o,N} - p_{o,P}) - T_{w,s} (p_{o,P} - p_{o,S})] - [T_{w,n} \frac{dp_{cow}}{dS_w} \Big|_n (S_{w,N} - S_{w,P}) - T_{w,s} \frac{dp_{cow}}{dS_w} \Big|_s (S_{w,P} - S_{w,S})] \\
 & - [\frac{k_{yy}(\lambda_w \gamma_w + \lambda_o \gamma_o) A_2}{\delta y} \Big|_n (z_{w,N} - z_{w,P}) - \frac{k_{yy}(\lambda_w \gamma_w + \lambda_o \gamma_o) A_2}{\delta y} \Big|_s (z_{w,P} - z_{w,S})] \\
 & + [T_{w,t} (p_{o,T} - p_{o,P}) - T_{w,b} (p_{o,P} - p_{o,B})] - [T_{w,t} \frac{dp_{cow}}{dS_w} \Big|_t (S_{w,T} - S_{w,P}) - T_{w,b} \frac{dp_{cow}}{dS_w} \Big|_b (S_{w,P} - S_{w,B})] \\
 & - [\frac{k_{zz}(\lambda_w \gamma_w + \lambda_o \gamma_o) A_3}{\delta z} \Big|_t (z_{w,T} - z_{w,P}) - \frac{k_{zz}(\lambda_w \gamma_w + \lambda_o \gamma_o) A_3}{\delta z} \Big|_b (z_{w,P} - z_{w,B})] + [\frac{q_w}{\rho_w} + \frac{q_o}{\rho_o}] \Delta V
 \end{aligned} \quad (17)$$

Here  $T_{it}$  implies the calculation of the transmissibility considering the total mobility  $\lambda$  and  $T_w$  refers to the transmissibility considering the mobility of the water phase  $\lambda_w$ . In equations (16) and (17) the superscript  $n+1$  is omitted for simplicity.

#### Newton-Raphson Method

Because there are nonlinearities in the discretized equations, the Newton-Raphson method was selected to linearize and to solve these equations. The main advantage of the method is its numerical stability compared with methods which use explicit discretization (Abou-Kassem *et al.*, 2006; Chen, 2007). For applying the Newton-Raphson method  $p_o^{n+1}$  and  $S_w^{n+1}$  were selected as primary variables. Thus, the system of equations to solve has the following form

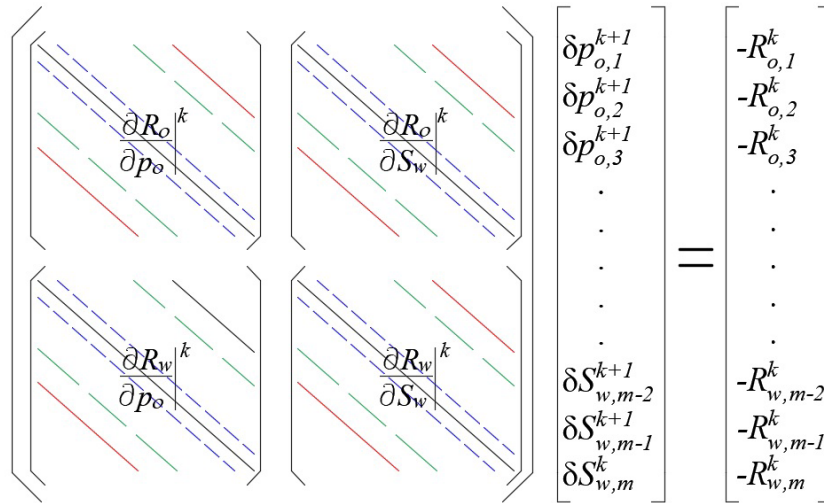
$$\begin{pmatrix} \frac{\partial R_o}{\partial p_o} \Big|_o^k & \frac{\partial R_o}{\partial S_w} \Big|_o^k \\ \frac{\partial R_w}{\partial p_o} \Big|_o^k & \frac{\partial R_w}{\partial S_w} \Big|_o^k \end{pmatrix} \begin{pmatrix} \delta p_o^{k+1} \\ \delta S_w^{k+1} \end{pmatrix} = \begin{pmatrix} -R_o^k \\ -R_w^k \end{pmatrix} \quad (18)$$

Matrix on the left of equation (18) is the Jacobian and superscript  $k$  is used to indicate the Newtonian iteration. The system written in extended form gives:

$$\begin{aligned}
 & \frac{\partial R_o(p_o, S_w)}{\partial p_{o,B}} \Big|_o^k \delta p_{o,B}^{k+1} + \frac{\partial R_o(p_o, S_w)}{\partial p_{o,S}} \Big|_o^k \delta p_{o,S}^{k+1} + \frac{\partial R_o(p_o, S_w)}{\partial p_{o,W}} \Big|_o^k \delta p_{o,W}^{k+1} + \frac{\partial R_o(p_o, S_w)}{\partial p_{o,P}} \Big|_o^k \delta p_{o,P}^{k+1} + \\
 & \frac{\partial R_o(p_o, S_w)}{\partial p_{o,E}} \Big|_o^k \delta p_{o,E}^{k+1} + \frac{\partial R_o(p_o, S_w)}{\partial p_{o,N}} \Big|_o^k \delta p_{o,N}^{k+1} + \frac{\partial R_o(p_o, S_w)}{\partial p_{o,T}} \Big|_o^k \delta p_{o,T}^{k+1} + \\
 & \frac{\partial R_o(p_o, S_w)}{\partial S_{w,B}} \Big|_o^k \delta S_{w,B}^{k+1} + \frac{\partial R_o(p_o, S_w)}{\partial S_{w,S}} \Big|_o^k \delta S_{w,S}^{k+1} + \frac{\partial R_o(p_o, S_w)}{\partial S_{w,W}} \Big|_o^k \delta S_{w,W}^{k+1} + \frac{\partial R_o(p_o, S_w)}{\partial S_{w,P}} \Big|_o^k \delta S_{w,P}^{k+1} + \\
 & \frac{\partial R_o(p_o, S_w)}{\partial S_{w,E}} \Big|_o^k \delta S_{w,E}^{k+1} + \frac{\partial R_o(p_o, S_w)}{\partial S_{w,N}} \Big|_o^k \delta S_{w,N}^{k+1} + \frac{\partial R_o(p_o, S_w)}{\partial S_{w,T}} \Big|_o^k \delta S_{w,T}^{k+1} = -R_o^k
 \end{aligned} \quad (19)$$

$$\begin{aligned}
& \left. \frac{\partial R_w(p_o, S_w)}{\partial P_{o,B}} \right|^k \delta p_{o,T}^{k+1} + \left. \frac{\partial R_w(p_o, S_w)}{\partial P_{o,S}} \right|^k \delta p_{o,S}^{k+1} + \left. \frac{\partial R_w(p_o, S_w)}{\partial p_{o,W}} \right|^k \delta p_{o,W}^{k+1} + \left. \frac{\partial R_w(p_o, S_w)}{\partial p_{o,P}} \right|^k \delta p_{o,P}^{k+1} + \\
& \left. \frac{\partial R_w(p_o, S_w)}{\partial p_{o,E}} \right|^k \delta p_{o,E}^{k+1} + \left. \frac{\partial R_w(p_o, S_w)}{\partial p_{o,N}} \right|^k \delta p_{o,N}^{k+1} + \left. \frac{\partial R_w(p_o, S_w)}{\partial p_{o,T}} \right|^k \delta p_{o,T}^{k+1} + \\
& \left. \frac{\partial R_w(p_o, S_w)}{\partial S_{w,B}} \right|^k \delta S_{w,T}^{k+1} + \left. \frac{\partial R_w(p_o, S_w)}{\partial S_{w,S}} \right|^k \delta S_{w,S}^{k+1} + \left. \frac{\partial R_w(p_o, S_w)}{\partial S_{w,W}} \right|^k \delta S_{w,W}^{k+1} + \left. \frac{\partial R_w(p_o, S_w)}{\partial S_{w,P}} \right|^k \delta S_{w,P}^{k+1} + \\
& \left. \frac{\partial R_w(p_o, S_w)}{\partial S_{w,E}} \right|^k \delta S_{w,E}^{k+1} + \left. \frac{\partial R_w(p_o, S_w)}{\partial S_{w,N}} \right|^k \delta S_{w,N}^{k+1} + \left. \frac{\partial R_w(p_o, S_w)}{\partial S_{w,T}} \right|^k \delta S_{w,T}^{k+1} = -R_w^k
\end{aligned} \tag{20}$$

Equations (19), (20) along with the residuals (16) and (17) are used to build the linear system as shown in Figure 2, where the subscript  $m$  refers to the total number of discrete volumes.



$$\begin{bmatrix}
\left. \frac{\partial R_o}{\partial p_o} \right|^k & \left. \frac{\partial R_o}{\partial S_w} \right|^k & \left. \frac{\partial R_w}{\partial p_o} \right|^k & \left. \frac{\partial R_w}{\partial S_w} \right|^k \\
\vdots & \vdots & \vdots & \vdots \\
\delta S_{w,m-2}^{k+1} & \delta S_{w,m-1}^{k+1} & \delta S_{w,m}^k & \vdots
\end{bmatrix}
\begin{bmatrix}
\delta p_{o,1}^{k+1} \\
\delta p_{o,2}^{k+1} \\
\delta p_{o,3}^{k+1} \\
\vdots \\
\delta S_{w,m-2}^{k+1} \\
\delta S_{w,m-1}^{k+1} \\
\delta S_{w,m}^k
\end{bmatrix}
=
\begin{bmatrix}
-R_{o,1}^k \\
-R_{o,2}^k \\
-R_{o,3}^k \\
\vdots \\
-R_{w,m-2}^k \\
-R_{w,m-1}^k \\
-R_{w,m}^k
\end{bmatrix}$$

**Figure 2.** Linear system equations for the primary variables  $p_o$  and  $S_w$ .

One of the main issues in this kind of problems is how to calculate the Jacobian elements and how to solve the resulting linear system. Both tasks are time consuming, therefore new techniques are needed to reduce the time used in doing these computational processes. In the next section details of the computational implementation that makes use of graphical processing units (GPUs) are presented in order to parallelize the construction of the Jacobian and the solution of the resulting linear system

### Computational implementation

In this section, the computational methodology used is briefly described to implement the algorithms provided by the numerical methods outlined in previous sections.

### CPU Implementation

First of all, the algorithms to be executed in an ordinary CPU were implemented for comparison purposes. The codes were written using the C++ language and the EIGEN library (Jacob and Guennebaud, 2016), the last one was used to simplify the array and matrices management and the solution of the linear systems of equations. The pseudocode of the main algorithm is shown in Figure 3.

In the first three lines of the pseudocode shown in Figure 3, all required variables and arrays are declared and initialized with adequate values, this includes the initial and boundary conditions, petrophysical values, size of the mesh, time step, etc. In line 4 the simulation



```

01 /* Initialization of all variables and initial data,
02    construction of all arrays to store field variables
03    and matrices and vectors of linear system */
04 WHILE (Time_step <= Total_time) DO
05     WHILE ( Delta_Sw < epsilon & Iteration < Max_iter) DO
06         Calculate oil components of Jacobian and Ro
07         Calculate water components of Jacobian and Rw
08         Build Jacobian matrix using the CRS format
09         Solve the linear system of equations using BICGSTAB
10     END WHILE
11     Update old variables
12     IF (!(Time_step % Frequency)) THEN
13         Save or print primary variables (po and Sw)
14     END IF
15 END WHILE
16 /* Free memory and finalize simulation */

```

**Figure 3.** Pseudocode of the main algorithm.

initiates and is carried out until the total number of time steps is reached. Inside this first cycle, another one implements the Newton-Raphson (NR) algorithm. This internal cycle starts in line 5 and is carried out until the norm of the change of the water saturation ( $|\delta S_w|$ ) is less than a prescribed value ( $\epsilon$ ) or the prescribed maximum number of iterations of the NR algorithm is reached. Lines 6 to 9 represent the main steps to solve the problem and use the highest percentage of CPU time. In lines 6 and 7 every entry of the Jacobian matrix is calculated, this means to calculate the discretized components of the residuals, equations (18) and (19), and their corresponding derivatives. It is worth mentioning that all derivatives are done numerically and first order forward finite differences are used to do so. Then in step 9 the Jacobian matrix is build using the Compressed Row Storage (CRS) format in order to take advantage of the sparseness of the matrix and to save memory. In the calculations, these three steps take around 8% of the total time. In line 9 the linear system is solved using the Biconjugate Gradient Stabilized (BICGSTAB) method algorithm which is contained in the EIGEN library. This step takes around 75% of the total CPU time. Once the NR algorithm has converged, all the required variables were updated to be used in the next time step, line 11. Finally, the solution (primary variables) were saved or printed every time the *Iteration* variable is divisible by a prescribed *Frequency*. This frequency will become important in the GPU implementation.

#### GPU Implementation

The implementation in CPU presented in the previous section is standard and do not have any complications. For the GPU implementation the

Compute Unified Device Architecture (NVIDIA, 2012) and the CUSP Library were used, which provides a high-level interface for manipulating sparse matrices and solving sparse linear systems (Maia and Dalton, 2016). The present implementation is almost done totally in GPU, which means that the amount of information exchange between CPU and GPU is relatively low. In this sense, the pseudocode of the main algorithm for GPU implementation is similar to the one shown in Figure 3. The following differences have to be mentioned: a) the cycle starting in line 4 require all the variables and arrays defined in lines 1-3, therefore a first exchange of information is done from CPU to GPU, however this is minimal due to the fact that the biggest arrays are constructed directly in the GPU; b) the operations in lines 6, 7, 8, 9 and 11 are all coded in CUDA, therefore, several kernel functions occur that are executed in the GPU device; c) the operation in line 13 requires a movement of information from GPU to CPU, however this is done only every time the *Iteration* is divisible by the *Frequency* and this can be just one time, for example when the simulation is finished, or when the user requires the information of the final solution.

The kernel functions are executed in parallel by threads. These threads are defined by global indexes that belong to a grid of blocks. The grid and block sizes are defined by the user. The grid can be defined for 1, 2 or 3 dimensions. Each block has a finite number of threads, usually up to 1024 thread count. The maximum grid size is given by the manufacturing specifications of each graphics card. All this features of modern GPUs can be consulted elsewhere in NVIDIA CUDA web site. Taking all this into account, it is only possible to efficiently parallelize numerical codes that do not exceed the number of threads



that can be executed in the grid of blocks. On the other hand, it is easy to parallelize functions that execute the same operations over the entries of arrays, since only the threads indexes have to be defined and this definition replaces each loop. As an example of this method, Figures 4 and 5 show an extract of the codes for calculating the Jacobian block corresponding to the residual  $R_o$  and its derivatives ( $\partial R_o / \partial p_o$ ), in CPU and GPU respectively.

In the function `jacobianCoeff_RoPo3D()` all the coefficients of Jacobian block  $\partial R_o / \partial p_o$  were calculated. The code is standard and is based in tridimensional arrays which contain some variables related to the Cartesian mesh for the numerical simulation. Therefore, three nested cycles occur, one cycle for each axis. In the most internal cycle, several functions are executed to carry out several numerical methods, among them: interpolations for initial relative permeability and saturations from centers of volumes to its faces (lines 5 and 6), calculation of relative permeability using data from tables (line 7), calculations of coefficients of the residual and its derivatives (lines 9 and 10), and the assembling of the corresponding block (line 11).

In the same way as in the Figure 4, in Figure 5 an extract of code of the kernel function is shown that implements the calculation of the Jacobian block  $\partial R_o / \partial p_o$ . The kernel function `jacobianCoeff_RoPo3D()` is executed in the GPU. The first thing to do is to determine the thread index, see lines 2-4. Using this index it is possible that each thread of the block in the grid, execute the operations defined in lines 5-12 concurrently. Line 5 is required to assure that the index is inside the limits of the arrays. Lines 6 to 12 consist of kernel functions, similar to the functions defined in CPU, see Figure 4, but using the index to perform each one of the numerical methods needed to calculate the corresponding block of the Jacobian matrix. These kernels are device functions that can only be executed by another kernel and are able to use the GPU memory (Sanders, 2010; NVIDIA, 2012). Two kind of memories were used: global memory to store the primary variables ( $S_w$  and  $p_o$ ), the properties of the porous media ( $k$ ,  $\phi$ , etc) and some other important arrays of the simulation; constant memory is used to store constant values, i.e, the viscosities, conversion factors and some tables of properties (relative permeability). Figure 6 shows schematically how the variables are stored within the GPU memory.

```

01 void jacobianCoeff_RoPo3D (*physical parameters as arguments) {
02     for (i=1; i<nx-1; i++){
03         for (j=1; j<ny-1; j++){
04             for (k=1; k<nz-1; k++){
05                 interpolatePermeability(k, k_e, k_w, k_n, k_s, k_t, k_b);
06                 interpolateSaturation(Sw, Sw_e, Sw_w, Sw_n, Sw_s, Sw_t, Sw_b);
07                 calculate_kro(Sw, kro_e, kro_w, kro_n, kro_s, kro_t, kro_b);
08 /* ... Some other calculations ... */
09                 F(Po)=Tr_e*(Po);
10                 F(Po+deltaPo)=Tr_e*(Po+deltaPo);
11                 Block_RoPo3D[3D(i,j,k)]=firstOrderDerivative(F(Po), F(Po+deltaPo), deltaPo);
12             }
13         }
14     }
15 }

```

**Figure 4.** Function to calculate the Jacobian block.

```

01 __global__ void jacobianCoeff_RoPo3D (*physical parameters as arguments) {
02     int i = threadIdx.x + blockIdx.x*blockDim.x;
03     int j = threadIdx.y + blockIdx.y*blockDim.y;
04     int k = threadIdx.z + blockIdx.z*blockDim.z;
05     if(i>0 && i < nx-1 && j > 0 && j < ny-1 && k > 0 && k < nz-1){
06         interpolatePermeability(k, k_e, k_w, k_n, k_s, k_t, k_b);
07         interpolateSaturation(Sw, Sw_e, Sw_w, Sw_n, Sw_s, Sw_t, Sw_b);
08         calculate_kro(Sw, kro_e, kro_w, kro_n, kro_s, kro_t, kro_b);
09 /* ... Some other calculations ... */
10         F(Po)=Tr_e*(Po);
11         F(Po+deltaPo)=Tr_e*(Po+deltaPo);
12         Block_RoPo3D[3D(i,j,k)]=firstOrderDerivative(F(Po), F(Po+deltaPo), deltaPo);
13     }
14 }

```

**Figure 5.** Kernel function to calculate the Jacobian block.

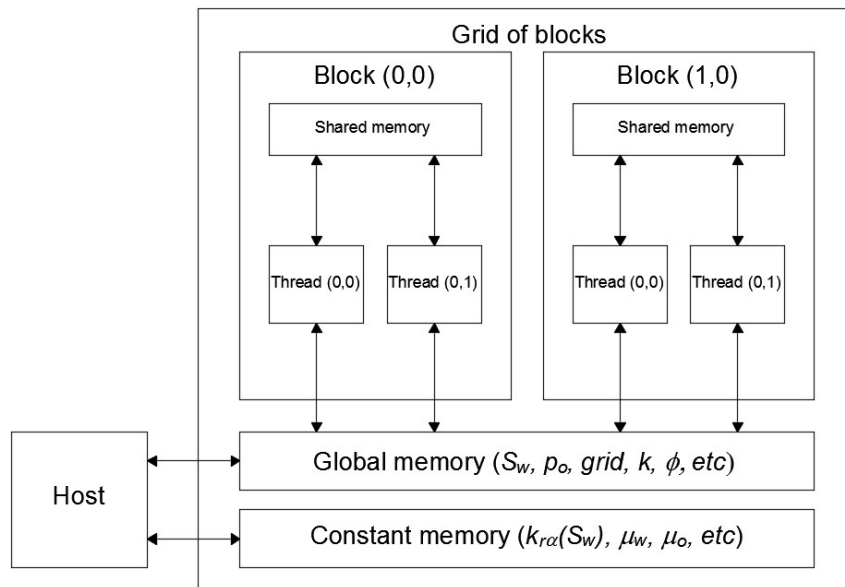


**Figure 6.** GPU memory used to store variables to build the Jacobian.

Finally, once the Jacobian components have been built, the linear system of equations is constructed in CRS format. This extra step is needed in order to use the algorithms of the EIGEN and CUSP libraries. Both libraries require a matrix in the CRS format and a right hand side (rhs) vector. The result is stored in another vector that contains the solution of the linear system.

### Numerical results

As a way to validate the numerical code, in this section numerical results obtained for three different cases are presented. Also numerical performance experiments were carried out to test computationally the parallel numerical code that is compared versus serial code.

#### Buckley Leverett

The Buckley-Leverett model describes the displacement of oil by water in an horizontal domain. This mathematical model is widely used in the validation of two phase fluid flow simulators, because it has an analytic solution for the water saturation profile. The hypothesis of the Buckley-Leverett model are:

- The displacement occurs at a one-dimensional medium.
- The porous media is isotropic.
- No effects of capillary pressure nor gravity forces are considered.
- There are no sources nor sinks.

- Water gets injected to a constant flow through the left boundary of the domain. Oil is produced on the right boundary at a constant pressure.

The parameters to carry out the simulation are shown in Table 1. Relative permeabilities  $k_{ra}(S_w)$  can be obtained from Chen *et al.* (2006).

In this paper a comparison of the analytical solution versus the solution obtained numerically is presented. The numerical parameters were selected as follows: to evaluate the derivatives within the Jacobian blocks increments of  $\Delta S_w = 1 \times 10^{-5}$  for water saturation and  $\Delta p_o = 0.1$  for the oil pressure were used. Stop criterion for leaving the Newton-Raphson loop was selected to:  $|\delta S_w| < 1 \times 10^{-5}$  and a fixed time step of 1 day

**Table 1.** Parameters to solve the Buckley-Leverett problem.

Property	Value
Length of domain ( $L_x$ )	1,000 (ft)
Absolute permeability ( $k$ )	100.0 (mD)
Porosity ( $\phi$ )	0.20
Water viscosity ( $\mu_w$ )	0.42 (cP)
Oil viscosity ( $\mu_o$ )	15.5 (cP)
Residual water saturation ( $S_{wr}$ )	0.40
Residual oil saturation ( $S_{or}$ )	0.18
Injection velocity ( $v_{inj}$ )	2.0E-06 (ft/s)
Production pressure ( $p_{out}$ )	1,000 (psi)

was chosen. The number of discrete volumes selected to study its effect in the solution were: 100, 500, 1,000, 5,000 and 10,000. The total time simulation was of 120 days and results are saved every 30 days. Table 2 shows a comparison between analytical and numerical solutions at some selected positions. As shown in this table as the number of volumes increases the relative error and the root mean square deviation (RMSD) respect to the analytical solution decreases.

Figure 7 shows the water saturation and pressure profiles obtained for 120 days of total simulation by using 10,000 discrete volumes. Results of the water saturation profile are congruent with the analytical solution (dashed line). This result indicates that the problem has been solved correctly.

**Table 2.** Numerical results obtained for the Buckley-Leverett problem.

Number of discrete volumes	Position $x$ (ft)	Simulation time (days)	Sw Numerical	Sw Analytical domain	Error %	RMSD At the whole
100	145	30	0.4721	0.4	18.033	0.01510
	275	60	0.4792	0.4	19.809	0.01590
	405	90	0.4801	0.4	20.037	0.01598
	535	120	0.4786	0.4	19.666	0.01875
500	145	30	0.42238	0.4	5.5942	0.01127
	275	60	0.42049	0.4	5.1216	0.01095
	405	90	0.40972	0.4	2.4295	0.01104
	535	120	0.40849	0.4	2.1213	0.01093
1,000	145	30	0.40784	0.4	1.9593	0.00987
	275	60	0.40399	0.4	0.99737	0.01027
	405	90	0.40080	0.4	0.19905	0.00981
	535	120	0.40056	0.4	0.13941	0.00962
5,000	145	30	0.40028	0.4	0.07096	0.00944
	275	60	0.39998	0.4	0.00525	0.00942
	405	90	0.39999	0.4	0.00170	0.00897
	535	120	0.40001	0.4	0.00150	0.00839
10,000	145	30	0.400130	0.4	0.03159	0.00916
	275	60	0.400020	0.4	0.00568	0.00917
	405	90	0.400001	0.4	0.00093	0.00881
	535	120	0.400001	0.4	0.00091	0.00827

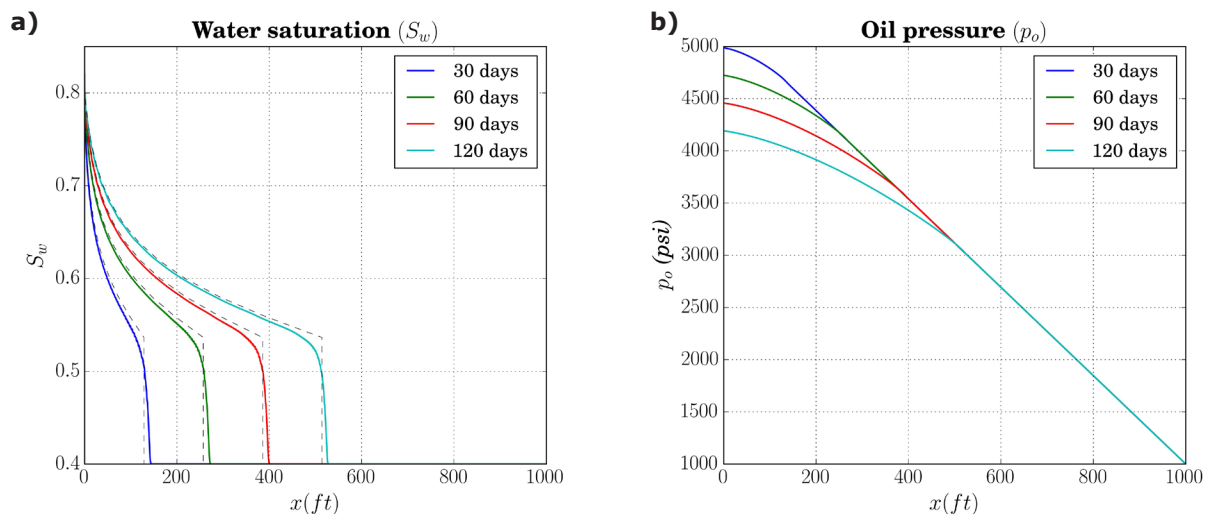


**Figure 7.** Results for 10,000 discrete volumes: a) Water saturation profile  $S_w$ , analytical solution (dashed line) versus numerical solution (continuous line); b) Oil pressure profile  $p_o$ .

### Five Spot

The model known as "Five Spot" describes the displacement of oil by water in an isotropic domain, in which a producer well and an injector well are placed in the opposite corners of the domain (See Figure 8). In the Five Spot conceptual model the follow assumptions are considered:

- The displacement occurs at a bidimensional domain.
- The porous media is isotropic.
- The effects of capillary pressure are considered.
- There are one source (injector well) and one sink (producer well).
- Gravity forces are neglected.

The parameters to carry out the simulation are shown in Table 3. Relative permeabilities  $k_{rq}$  ( $S_w$ ) and capillary pressure  $p_{cow}$  can be obtained from Chen *et al.* (2006).

**Table 3.** Parameters to solve the Five Spot problem (Chen *et al.*, 2006).

Property	Value
Size of domain ( $L_x \times L_y$ )	1,000 x1,000 (ft)
Absolute permeability ( $k$ )	100.0 (mD)
Porosity ( $\phi$ )	0.20
Water viscosity ( $\mu_w$ )	0.096 (cP)
Oil viscosity ( $\mu_o$ )	1.14 (cP)
Residual water saturation ( $S_{wr}$ )	0.22
Residual oil saturation ( $S_{or}$ )	0.20
Injection pressure ( $p_{wb}^{in}$ )	3,700 (psi)
Production pressure ( $p_{wb}^{out}$ )	3,500 (psi)

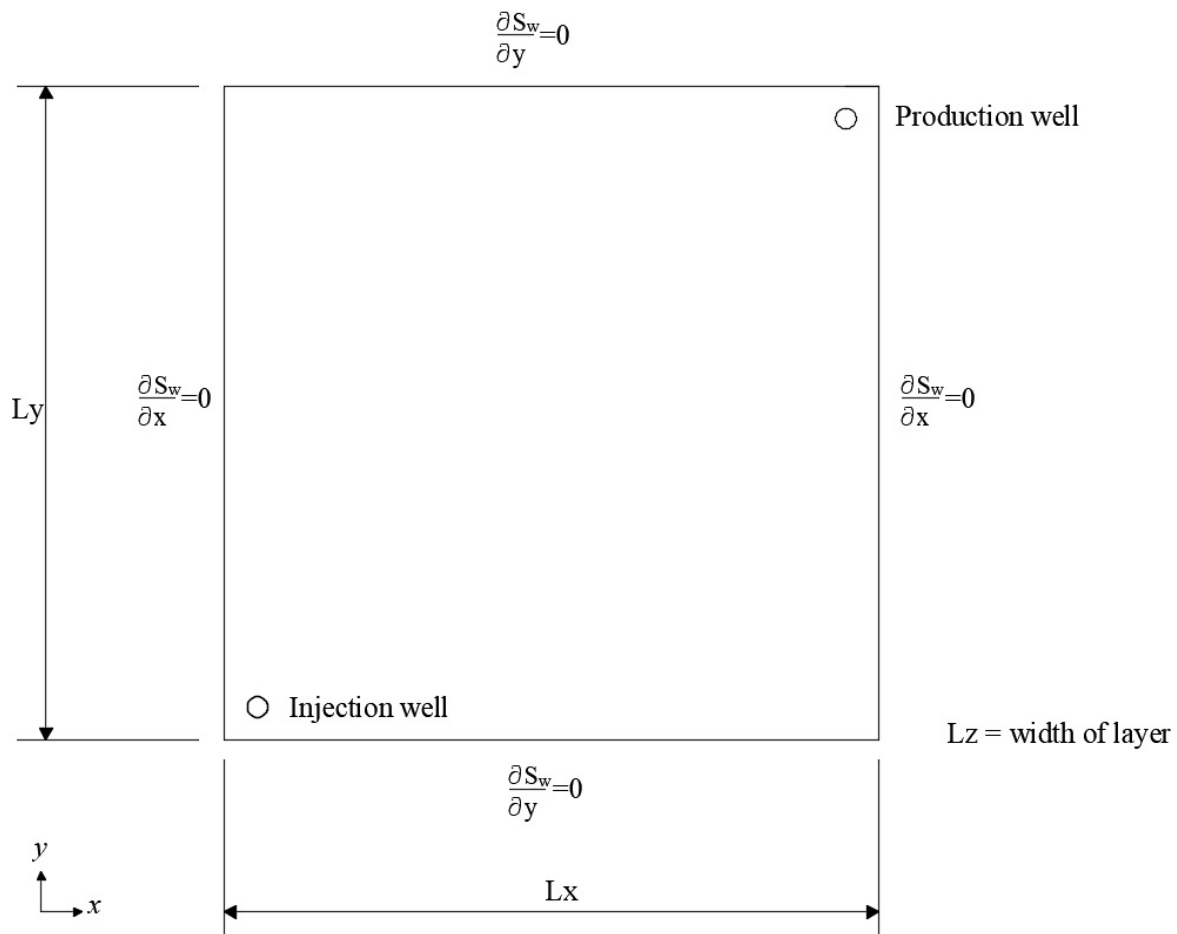


**Figure 8.** Five Spot physical model.

For this problem the total time simulation was selected to 8,000 days and the results are reported every 500 days. Numerical parameters are the same to those in the Buckley-Leverett problem. Because there is no analytical solution for this problem, it is validated with the results reported by Chen *et al.* (2006). Figure 9 a) shows the production of water and oil in reservoir barrels per day (RB/day) throughout the simulation time. In this figure it can be seen that the results reported by Chen *et al.* (2006) and those obtained in this work have a similar qualitatively behavior. The difference between curves may be due to the numerical techniques used, since Chen *et al.* (2006) used an adaptive time step with an IMPES scheme. The RMSD obtained for the production curves are 43.88 and 137.94 for oil and water production, respectively. In Figure 9 b) fractional flow ( $F_w$ ) curves are compared. It can be appreciated that the water cut happens after 1,000 days of simulation, which is almost the same result reported by Chen *et al.* (2006).

To verify the solution shape two more simulations were carried out, one considering 30x30 mesh size of and another using 90x90 volumes. Values obtained for RMSD using 30x30 volumes were 41.97 and 135.44; while by using 90x90 volumes were 41.02 and 134.82, for oil and water production respectively.

Figure 10 shows the water saturation profiles at different simulation times in the whole numerical domain. This figure is presented in order to clarify how the waterfront sweeps the oil from the porous medium.

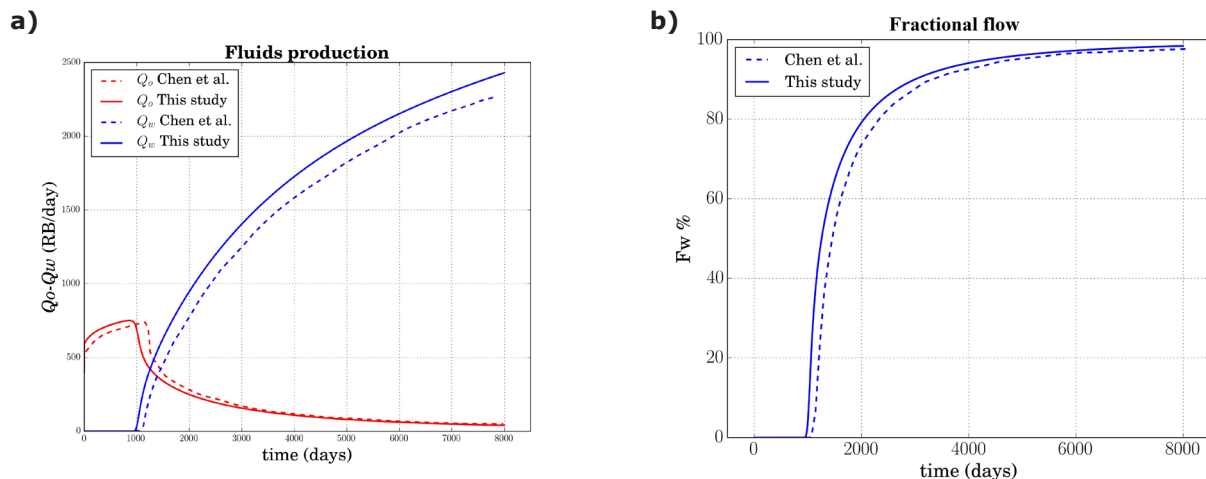
#### The seventh SPE project

The seventh SPE project is a benchmark that describes the water injection and oil production

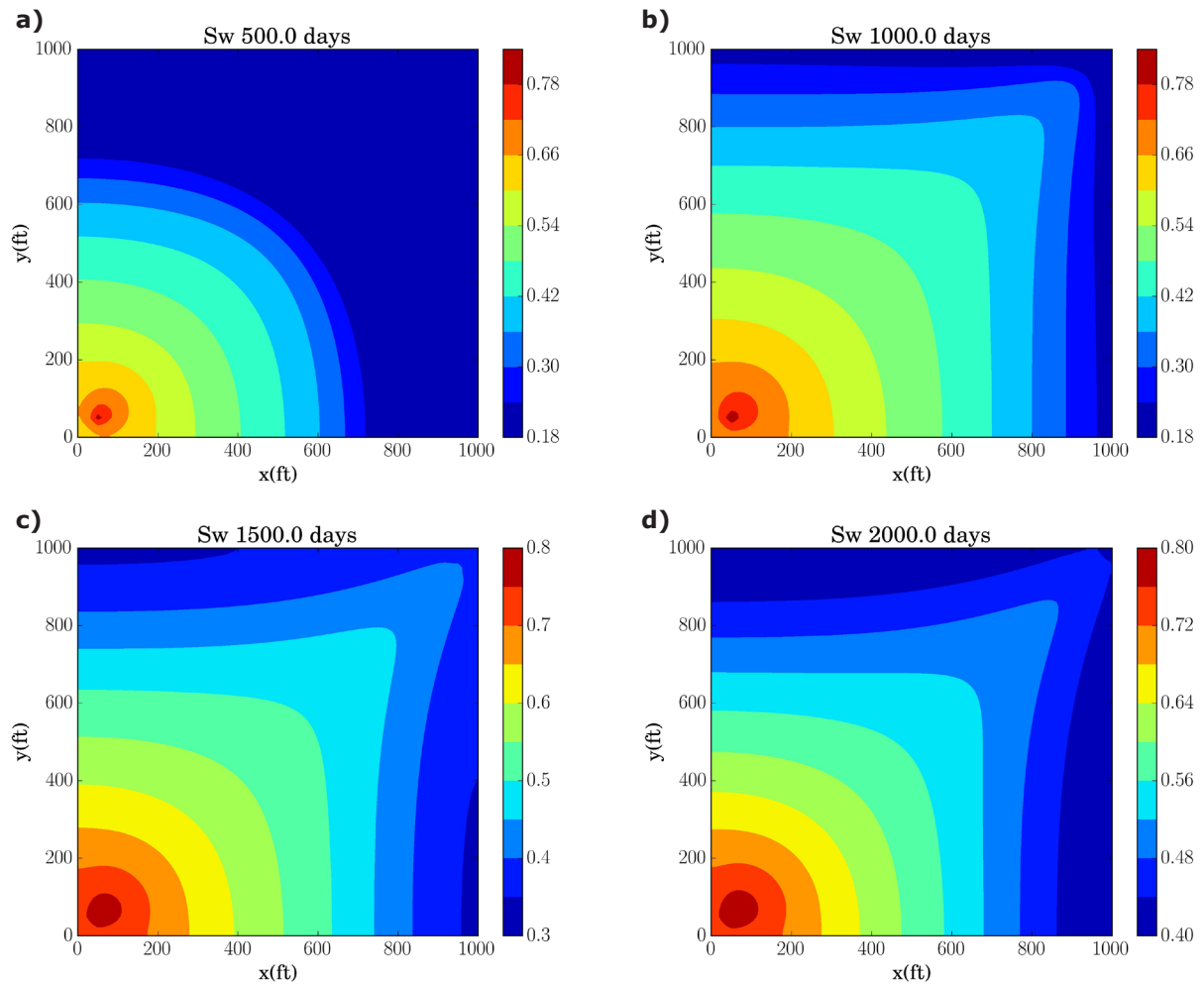
using horizontal wells, this problem was adapted by Nghiem *et al.* (1991) and Chen *et al.* (2006) for two-phase fluid flow. In the present case capillary pressure and gravity forces were considered. Therefore equations (10) and (14) are used without any modification.

To solve this problem the SPE proposes a mesh of 10x10x7 (Figure 11). This mesh is refined to the  $y$  axis center, in order to place the injection and production wells. The length of the blocks in the  $x$  axis are uniform and equal to 300 *ft* ( $\delta x = 300 *ft*). For the length of the blocks in the  $y$  axis, the distribution is as follows:  $\delta y_1 = \delta y_9 = 620 *ft*,  $\delta y_2 = \delta y_8 = 400 *ft*,  $\delta y_3 = \delta y_7 = 200 *ft*,  $\delta y_4 = \delta y_6 = 100 *ft* and  $\delta y_5 = 60 *ft*. For the  $z$  axis  $\delta z_k = 20 *ft* for  $k_{1,2,3,4}$ ,  $\delta z_5 = 30 *ft* and  $\delta z_k = 50 *ft* were used. Injection well is placed in the layer  $\delta z_6$ , at the center of the axis  $y$  and it crosses all the blocks in the  $x$  axis. Production well is placed in the layer  $\delta z_1$ , at the center of the axis  $y$  and it crosses only the blocks  $\delta x_{6,7,8}$  in the  $x$  axis. Parameters to execute the simulation are shown in Table 4. Relative permeabilities  $k_{rg}(S_w)$ , capillary pressure  $p_{cow}(S_w)$ , and initial conditions can be obtained from Nghiem *et al.* (1991).$$$$$$$$$

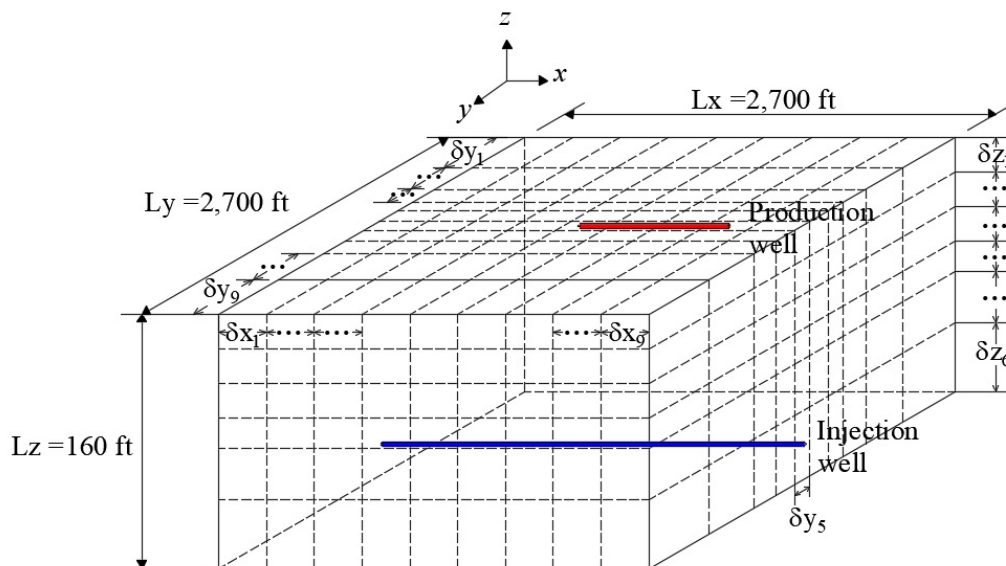
For this problem the total simulation time was selected to be 1,500 days and results are reported every 100 days. Results are validated by comparing production curves reported by Chen *et al.* (2006). Figure 12 a) shows the oil production in stock tank barrels per day (STB/day) during the entire simulation time. It can be noted that the results are qualitatively similar to those reported by Chen *et al.* (2006), although the curve reported by them declines slightly faster. The accumulated oil production curves are also compared, these results are shown in Figure 12 b).



**Figure 9.** Results obtained using 10x10 discrete volumes: a) water and oil productions  $Q_w$ - $Q_o$  in reservoir barrels per day (RB/day); b) fractional flow  $F_w$  (%).



**Figure 10.** Water saturation profiles for different simulation times using a 90x90 volume.

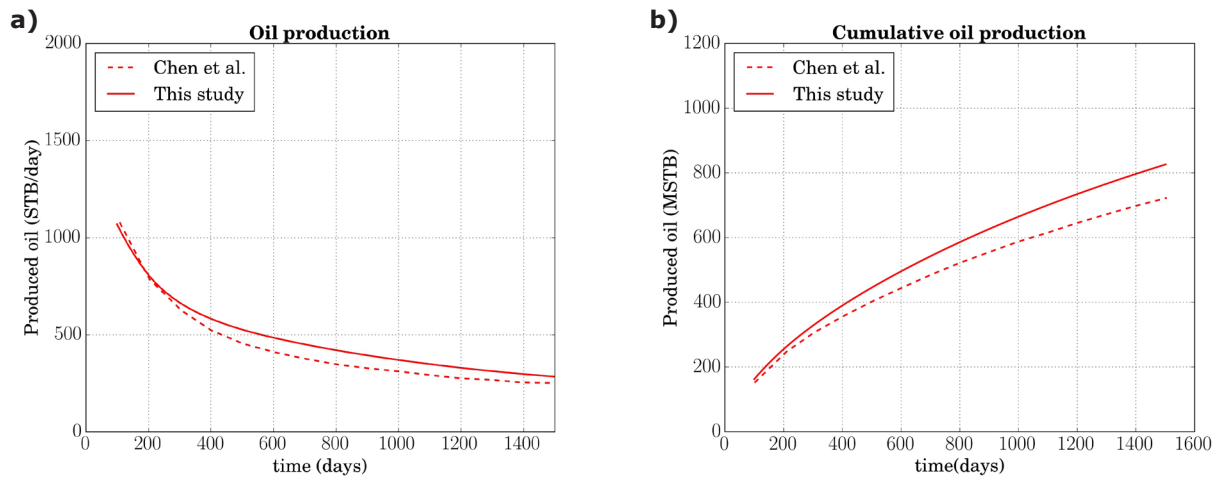


**Figure 11.** Seventh SPE project physical model.



**Table 4.** Parameters to solve the Seventh SPE project (Nghiem *et al.*, 1991).

Property	Value
Size of domain ( $L_x \times L_y \times L_z$ )	2,700 x 2,700 x160 (ft)
Absolute permeability ( $k_x, k_y, k_z$ )	(300.0, 300.0, 30.0) (mD)
Porosity ( $\phi$ )	0.20
Water viscosity ( $\mu_w$ )	0.96 (cP)
Oil viscosity ( $\mu_o$ )	0.954 (cP)
Residual water saturation ( $S_{wr}$ )	0.22
Residual oil saturation ( $S_{or}$ )	0.0
Injection pressure ( $p_{wb}^{in}$ )	3,651.4 (psi)
Production pressure ( $p_{wb}^{out}$ )	3,513.6 (psi)

**Figure 12.** Results obtained using 10X10X7 discrete volumes: a) Oil production (STB/day); b) Cumulative oil production (MSTB).

The small difference observed in Figures 12, may be due to implementations of the numerical method and conversion factor used for the STB; in the present work the STB conversion factor from Nghiem *et al.* (1991) was used. It should be noted that this problem was solved only with the grid size proposed by Nghiem *et al.* (1991), as it is indicated by this benchmark. The RMSD obtained in this problem is 55.77 for the oil production values and 68.08 for cumulative oil production. In order to know the behavior of the fluids flow in the layer where the production well is placed. Figure 13 shows the saturation profiles  $S_w$  in this layer for six selected simulation times by using the grid size proposed by Nghiem *et al.* (1991). For the saturation profiles belonging to 100 and 300 simulation days, it is noted that the water has begun to sweep the oil present in the layer forming a “water feather”. For the 1,200 and 1,500 profiles the water feather has spread out to more than a half the domain. This means that about 40% of the oil present in the layer has already been produced.

#### Numerical performance experiments

In order to analyze the performance of the numerical code, the five spot water injection problem was selected. Numerical parameters selected were:  $\Delta S_w = 1 \times 10^{-5}$  for water saturation and  $\Delta p_o = 1 \times 10^{-3}$  for oil pressure. Stop criterion for leaving the Newton-Raphson loop was selected to:  $|\delta S_w| < 1 \times 10^{-3}$  and a fixed time step of 0.01 day was chosen; results are saved every 1.0 day. 10 days were selected for the total simulation time.

Numerical results presented in this section were obtained by executing our numerical code in a workstation with a single processor Intel (R) i7 (R) CPU 3820 3.60 GHz, 16 Gigabytes of RAM and an NVIDIA Tesla C2075 (R) GPU with 448 cuda-cores and 6 Gigabytes of dedicated memory.

Table 5 shows the average run-time for each Newton-Raphson step. The Jacobian run-

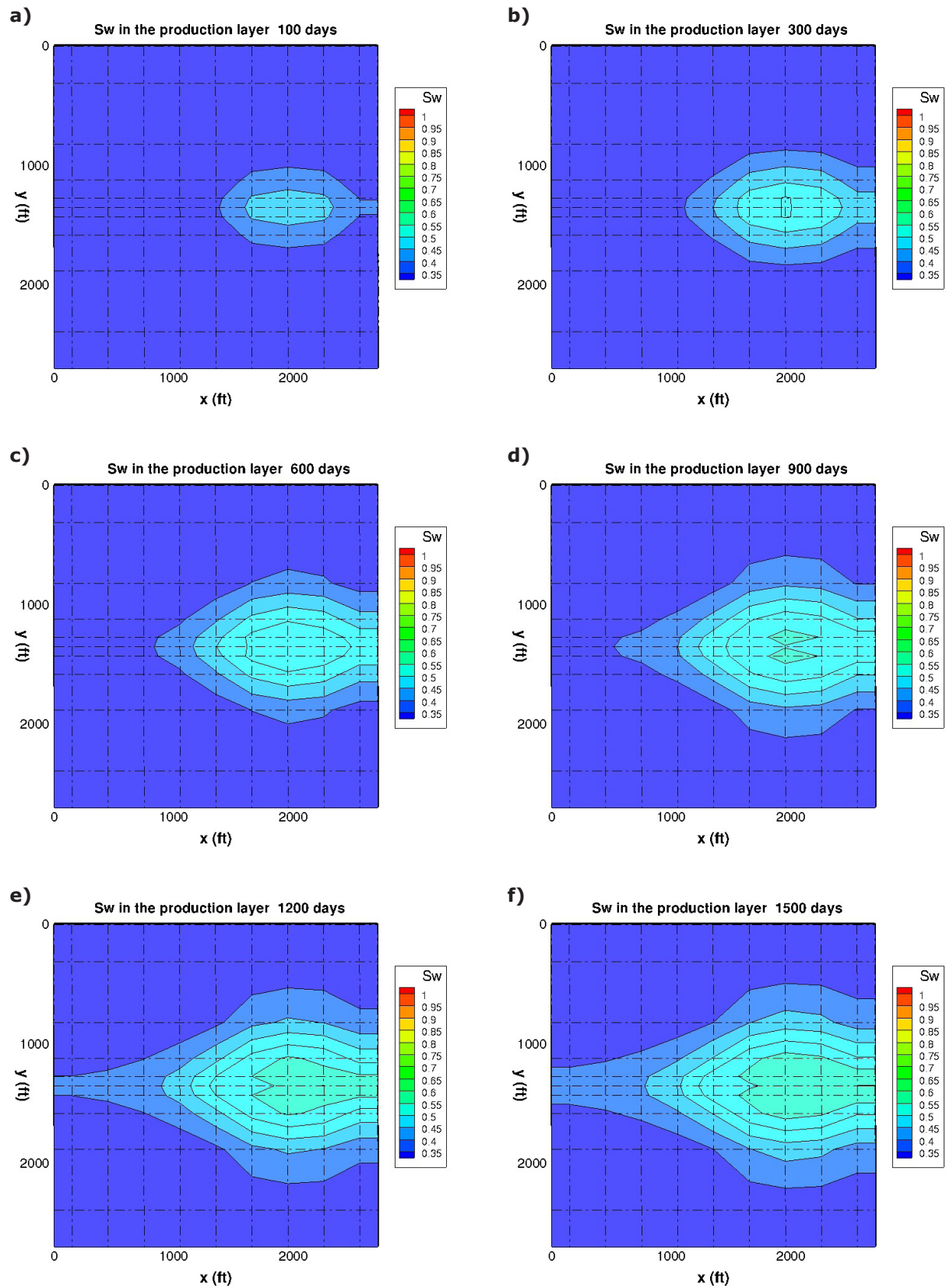


**Figure 13.** Water saturation profiles in the production layer for different simulation times.

time increases considerably when the number of volumes is bigger. As an example, 0.796 s were spent when volumes were 550x550 in CPU, while only 0.0379 s were used on the GPU that means 21x of speed up. This result is a considerable save of computation time taking into account that this procedure has to be repeated every Newton iteration.

Most authors indicate about 75% computation time is consumed in the solution of the system of linear equations. For solving the linear equations system, BICGSTAB solver without a preconditioner was used. This solver is already included in EIGEN and CUSP libraries (Jacob and Guennebaud, 2016; Maia and Dalton, 2016). Run times are shown in Table 6. Results indicate that CPU is faster than GPU when linear system is small (45,000 unknowns). When the linear system increases from 45,000 to 125,000 unknowns the computing time using the GPU is less than CPU. For a system with 605,000 unknowns, the maximum speed up is achieved (2.207x).

In a numerical code developed with GPU without graphics in real time, numerical results always have to be transferred from GPU to CPU for later processing. This process is computationally expensive because it has to be carried out each time step or when the user requires it.

The time measured for this operation was from  $1.69 \times 10^{-05}$  to 0.101 seconds, for the 30x30 and 550x550 number of volumes, respectively. For this reason real speed up must be quantified when the whole numerical code has finished. Figure 14 shows run time and speed up for executing the whole code. In this figure can be noted GPU is slower than CPU when the problem is executed with few volumes. In the other hand, GPU speed up increases if the number of nodes for executing the problem increases. For executing the numerical code with 302,500 blocks (550x550 number of volumes) 3.0x of speed up is achieved, that is, the total run time for the CPU was 6.8 days whereas for the GPU it was only 2.26 days. It is worth mentioning that in this case the information transfer GPU-CPU does not have a considerable effect, since it was executed only 10 times. It should be kept in mind that this is a benchmark problem, therefore it is not necessary to use a bigger grid size to solve it adequately.

## Conclusions

Sequential and parallel implementations of a fully implicit simulator for waterflooding process have been presented. Both implementations were validated with three different benchmarks and similar results were obtained in comparison with other authors and in comparison with analytical

**Table 5.** Average run-time obtained to compute the Jacobian.

Number of volumes	CPU run-time (s)	GPU run-time (s)	Speed up (x)
30x30	0.00284	0.00084	3.38x
90x90	0.02340	0.00164	14.26x
150x150	0.07141	0.00311	22.96x
250x250	0.15049	0.00754	19.95x
550x550	0.79686	0.037937	21.00x

**Table 6.** Average run-time obtained to solve the linear equations system.

Number of volumes	Unknowns number	CPU run-time (s)	GPU run-time (s)	Speed up (x)
30x30	1,800	0.007599	0.21234	0.035x
90x90	16,200	0.19308	0.85252	0.226x
150x150	45,000	0.98792	1.0727	0.9209x
250x250	125,000	4.3418	2.7515	1.570x
550x550	605,000	29.408	13.32	2.207x

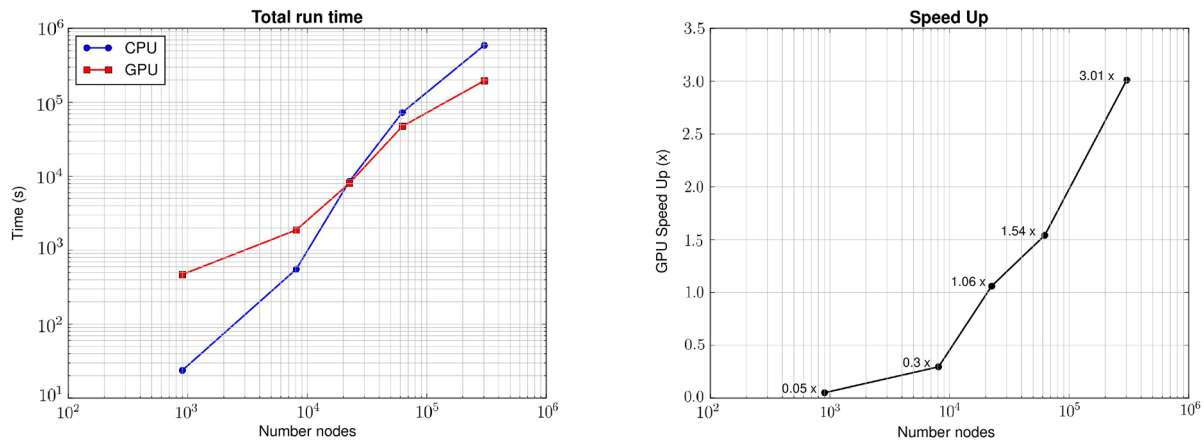


**Figure 14.** Numerical performance: a) CPU & GPU total run-time and b) GPU speed up.

solutions. The strategy of parallelization allows to reduce the calculation time of the Jacobian matrix, resulting from the Newton-Raphson method, using the architecture of the GPUs. Numerical results indicate that the GPU implementation reach until 22.9 times faster than the CPU counterpart for the finest mesh. On the other hand, the solution of the final linear system was also carried out in the GPU. A speed up of this step of 2.2 for the finest mesh was obtained. In total, taking into account the construction of the Jacobian matrix, the solution of the linear system and the exchange of information between CPU and GPU, gave a total speed up to 3. As expected, this speed up can be improved as the number of unknowns is incremented, however, the limited number of threads and memory of GPUs is a first obstacle to go forward. Even though the libraries used for solving the linear systems are optimized, they need to be improved with special preconditioners in order to obtain better results in terms of CPU and GPU time, and pair the 22x of speed up that was achieved in the present best calculation of Jacobian matrix. On the other hand, the GPU used in this work is not the newest one in the market, in such a way that a limitation occurs by the number of CUDA cores (448) and the memory (6GB) of the hardware; however, as can be seen, as the size of the problem increase, the speed up improves, therefore if, for example a GPU Tesla K40m (2880 CUDA cores and 12 GB in memory) is used better results can be expected. Finally, the present strategy can be used for several number of GPUs along with domain decomposition methods; this allows to increase even more the size of the problem (to several millions of unknowns) and as a consequence the speed up will be improved. Of course, this

requires better solvers for the linear systems, for example geometric or algebraic multigrid methods.

### Acknowledgments

V. Leonardo Teja-Juárez acknowledges the financial support from Consejo Nacional de Ciencia y Tecnología (CONACYT, MX) with the scholarship number 327261. Special thanks to my tutor committee: PhD. Ismael Herrera Revilla and PhD. Simon Lopez Ramirez for their valuable comments and advice during the development of this work.

### References

- Abou-Kassem J.H., Farouq-Ali S., and Islam M.R., 2006, Petroleum Reservoir Simulations: a basic approach. Gulf Publishing Company, Texas, pp 445.
- Anciaux-Sedrakian A., Eaton J., Gratien J., Guignon T., Havé P., Preux C., Ricois O., and others, 2015. Will GPGPUs be finally a credible solution for industrial reservoir simulators? in SPE Symposium on Reservoir Simulation. Houston, Texas, 23-25 February.
- Chen Z., 2007, Reservoir simulation: mathematical techniques in oil recovery. SIAM, Philadelphia, pp 219.
- Chen Z., Huan G., and Ma Y., 2006, Computational methods for multiphase flows in porous media. SIAM, Philadelphia, pp 521.
- de la Cruz, L.M. and Monsivais D., 2014, Parallel numerical simulation of two-phase flow

- model in porous media using distributed and shared memory architectures. *Geofísica internacional*, 53(1):59–75.
- Dogru A.H., Fung L.S., Middya U., Al-Shaalan T.M., Pita J.A., HemanthKumar K., Su H., Tan J.C., Hoy H., Dreiman W., 2009, A next-generation parallel reservoir simulator for giant reservoirs, In SPE/EAGE Reservoir Characterization & Simulation Conference, Abu Dhabi, United Arab Emirates, 19-21 October.
- Herrera I. and Pinder G.F., 2012, Mathematical modeling in science and engineering: An axiomatic approach. John Wiley & Sons, New Jersey, pp 243.
- Jacob B., and Guennebaud G., and others, 2016, template library for linear algebra, EIGEN C++, Web page: <http://eigen.tuxfamily.org>.
- Killough J., Bhogeswara R., and others, 1991, Simulation of compositional reservoir phenomena on a distributed-memory parallel computer. *Journal of Petroleum Technology*, 43(11):1–368.
- Lake L.W., 1989, Enhanced Oil Recovery. Prentice Hall, New Jersey, pp 550.
- Latil M., 1980, Enhanced oil recovery. Éditions Technip, Paris, pp 239.
- Li R. and Saad Y., 2013, GPU-accelerated preconditioned iterative linear solvers. *The Journal of Supercomputing*, 63(2):443–466.
- Liu H., Wang K., Chen Z., Jordan K., Luo J., Deng H., and others, 2015, A parallel framework for reservoir simulators on distributed-memory supercomputers, in SPE/IATMI Asia Pacific Oil & Gas Conference and Exhibition. Bali, Indonesia, 20-22 October
- Liu H., Yu S., Chen Z., 2013, Development of algebraic multigrid solvers using GPUs, in SPE Reservoir Simulation Symposium, The Woodlands, Texas, 18-20 February.
- Ma Y. and Chen Z., 2004, Parallel computation for reservoir thermal simulation of multicomponent and multiphase fluid flow. *Journal of Computational Physics*, 201(1):224–237.
- Maia F., and Dalton S., and others, 2016, Generic parallel algorithms for sparse matrix and graph computations, CUSP, Web page: <http://cusplibrary.github.io/>.
- Mukundakrishnan K., Esler K., Dembeck D., Natoli V., Shumway J., Zhang Y., Gilman J.R., Meng H., and others, 2015, Accelerating tight reservoir workflows with GPUs, in SPE Symposium on Reservoir Simulation. Houston, Texas, 23-25 February.
- Nghiem L., Collins D.A., Sharma R., 1991, Seventh SPE comparative solution project: Modelling of horizontal wells in reservoir simulation, in SPE Symposium on Reservoir Simulation, Anaheim, California, 17-20 February.
- NVIDIA, 2012, NVIDIA CUDA C Programming Guide, Version 4.2, Web page: <http://docs.nvidia.com/cuda/cuda-c-programming-guide>.
- Peaceman D.W., 1977, Fundamentals of numerical reservoir simulation. Elsevier, Texas, pp 176.
- Sanders J., and Kandrot E., 2010, CUDA by Example: An Introduction to General-Purpose GPU Programming. Addison-Wesley Professional, Boston, pp 290.
- Shiralkar G.S., Stephenson R., Joubert W., Lubeck O., van Bloemen Waanders B., 1998, Falcon: A production quality distributed memory reservoir simulator. *SPE Reservoir Evaluation & Engineering*, 1(05):400–407.
- Trapeznikova M.A., Churbanova N.G., Lyupa A.A., and Morozov D.N., 2014, Simulation of multiphase flows in the subsurface on GPU-based supercomputers. *Parallel Computing: Accelerating Computational Science Engineering (CSE)*, *Advances in Parallel Computing*, 25:324–333.
- Wang K., Liu H., and Chen Z., 2015, A scalable parallel black oil simulator on distributed memory parallel computers. *Journal of Computational Physics*, 301:19–34.
- Yu S., Liu H., Chen Z., Hsieh B., Shao L., 2012, GPU-based parallel reservoir simulation for large-scale simulation problems, in SPE Europec/EAGE Annual Conference, Copenhagen, Denmark, 4-7 June.